Accepted Manuscript

International Journal of Computational Methods

Article Title:	A Viscous Elasto-Plastic SPH Model for Long-Distance High-Speed Landslide
Author(s):	Wentao Zhang, Chuanqi Shi, Yi An, Shihao Yang, Qingquan Liu
DOI:	10.1142/S0219876218460118
Received:	01 January 2018
Accepted:	20 April 2018
To be cited as:	Wentao Zhang *et al.*, A Viscous Elasto-Plastic SPH Model for Long-Distance High-Speed Landslide, *International Journal of Computational Methods*, doi: 10.1142/S0219876218460118
Link to final version:	https://doi.org/10.1142/S0219876218460118

International Journal of Computational Methods

A Viscous Elasto-Plastic SPH Model for Long-Distance High-Speed Landslide

Wentao Zhang, Chuanqi Shi, Yi An and Shihao Yang

Laboratory for Mechanics of Fluid-Solid Coupling Systems, Institute of Mechanics, Chinese Academy of Sciences,
Beijing, China
zhangwentao@imech.ac.cn

Qingquan Liu

Department of Aero, Beijing Institute of Technology,
Beijing, China
liuqq@bit.edu.cn

Received (Day Month Year)
Revised (Day Month Year)

In the landslide induced debris flow problem, the soil slope experiences three stages: slope instability, debris flow and deposition. This study develops a three-dimensional smoothed particle hydrodynamics model which adopts elasto-plastic viscous constitutive relation to simulate this complex process. The Drucker–Prager model with non-associated plastic flow rules is implemented for slope instability and deposition and constant viscosity is used for propagation stage. The model is validated with laboratory dry-granular dam break experiments. Good agreement is found between the simulated results and the laboratory data on both the shape evolution and the velocity field. Then we use the model to study the Yigong avalanche after detailed discussion of model parameter, the time of duration, deposited scope and estimated velocity essentially agree with site survey. Thus the model is able to simulate instability and flow of dense granular materials at both experimental and field scale, it could provide a powerful tool for the landslide induced debris flow study.

Keywords: granular solid regime; granular liquid regime; viscous elasto-plastic model.

1. Introduction

Landslides, avalanches and debris flows are mass transport processes which contain large quantities of granular materials. Those processes often threat critical infrastructure and human life because of their enormous energy. Thus, building an effective numerical model is of great importance to hazard forecasts and disaster mitigation. Granular avalanches can be divided into three phases: initiation, transportation and deposition. Granular materials are mainly in solid-like regime in initiation and deposition stage, while they behave more fluid-like in transportation stage. Granular interact mainly by friction in granular solid state, researchers often adopt elasto-plastic constitutive relation to describe it. For a granular liquid, granular inter with others through friction as well as collision. The so-called μ(I) rheology was widely adopted in granular liquid regime, it described many phenomena successfully [Andreotti et al. (2013)].

The most widely used numerical method to describe large-scale geological disaster is shallow-type model. However, shallow-type model is hard to take granular material's constitutive relation in different stage into consideration [Gray and Edwards (2014)]. And granular avalanche doesn't satisfy Long wave assumption in initiation stage. Lastly, the velocity vertical against ground can't be ignored as in shallow-type model when there are abrupt changes in slope angle [Denlinger and Iverson (2004)]. The discrete element method (DEM) is also often used as a special numerical method to study granular motion [Huang et al. (2012)]. Although DEM could overcome the deficiencies of shallow-type method, this approach is computationally expensive. Moreover, stiffness parameter and damp parameter in DEM need to be calibrated by back analysis as they can't be directly obtained from experiments. In recent years, three-dimensional continuum model which take granular material's constitutive relation into consideration are got more and more attention [Martin et al. (2017); Holsapple (2013); Andrade et al. (2012)]. This type of method can avoid the aforementioned problems encountered in shallow-type model and DEM.

As for numerical approach, mesh based numerical methods, such as finite-element method (FEM) and finite-difference method (FDM), are usually employed to study slope stability as the condition in initiation stage [Griffiths and Marquez (2007); Zhang et al. (2013)]. However, those methods may suffer from severe mesh distortion problem in dealing with transportation stage of granular avalanche. Oppositely, mesh-free methods, such as smoothed particle hydrodynamics (SPH) and material point method (MPM), are very fit to investigate granular avalanche problem which accompanied by large deformations and free surface [Garg and Pant (2018)]. There are a lot of researches apply mesh-free methods to simulate motion of granular media in recent years. As for the consideration of constitutive model, elasto-plastic models are usually adopt for slope stability [Bui et al. (2008); Chen and Qiu (2014)]. While for researches focus on propagation of granular avalanche, a number of researchers still use classical Bingham rheology [Huang et al. (2012); Hu et al. (2015)]. Some models begin to employ μ(I) rheology borrowed from dense granular flow theory [Pahar and Dhar (2017); Xu et al. (2017)]. Until now, there are very few models able to describe the behavior of granular avalanche at both initiation phase and propagation phase. Although it begin to appear such models in recent two years, they are confined to 2D case in experimental scale owing to complex numerical implementation and high computational cost [Dunatunga and Kamrin (2015)].

The hypermobility behaviors of granular avalanche are still poorly understood and fiercely debated in the world. The runout efficiency, defined as the ratio of runout distance to initial height, is far greater than the simple estimation through friction coefficient of soil in the landslide [Lucas et al. (2014)]. Numerous mechanisms have been proposed to explain this phenomenon, such as excess pore pressure [Iverson (1997)], acoustic fluidization [Melosh (1979)] and fragmentation spreading [Davies et al. (1999)]. Although the numerical result of three-dimensional continuum models which take granular material's constitutive relation into consideration matched well with experimental data by use of measured parameters, it's not answered yet whether those methods can be applied to granular avalanche at field scale and does not need to calibrate parameter like shallow-type

model. Thus, an elasto-plastic viscous model is developed and then verified by experiments. Finally, this model is applied to study Yigong avalanche in Tibet, China.

This paper is organized as follows. The governing equations and SPH numerical scheme are presented in section 2. The experimental setup are firstly described and then detailed comparisons are made between numerical result and experimental data in section 3. Yigong avalanche in Tibet, China is studied and parameters selection are discussed in detail in section 4. Concluding remarks are presented in the last section.

2. The Elasto-Plastic Viscous Model

2.1. *Mathematical model*

Mass and momentum conservation are chosen as governing equations as follows.

$$\frac{\mathrm{D}\rho}{Dt} = -\rho \frac{\partial v^{\alpha}}{\partial x^{\alpha}} . \tag{1}$$

$$\frac{\mathrm{D}v^{\alpha}}{Dt} = \frac{1}{\rho}\frac{\partial \sigma^{\alpha\beta}}{\partial x^{\beta}} + f^{\alpha} . \tag{2}$$

where α, β denote the Cartesian components x, y, z with the Einstein convention applied to repeated indices; ρ is soil density; v is soil velocity; f^{α} is the component of acceleration caused by external force, which is the gravitational acceleration in this work; σ represents the total stress tensor of soil and it could be divided into elasto-plastic stress and viscous stress.

In granular solid regime, granular motion is mainly controlled by elasto-plastic stress. The elasto-plastic stress is got through stress-strain relationship

$$\frac{D\sigma_{epi}{}^{\alpha\beta}}{Dt} = 2G\dot{e}_i^{\alpha\beta} + K\varepsilon_i^{\gamma\gamma}\delta_i^{\alpha\beta} - \dot{\lambda}_i\left[3\alpha_{\psi}K\delta^{\alpha\beta} + \frac{G}{\sqrt{J_2}}s_i^{\alpha\beta}\right]. \tag{3}$$

where $\dot{\lambda}$ is the rate of change of plastic multiplier, it influence the magnitude of plastic strain a lot, $s_i^{\alpha\beta}$ is the deviatoric shear stress rate tensor, $\dot{e}_i^{\alpha\beta}$ is the deviatoric shear strain rate tensor; δ is Kronecker's delta, $\varepsilon_i^{\gamma\gamma}$ is the sum of three principal strain rates; K and G are, respectively, the elastic bulk modulus and the shear modulus, which are related to the Young's modulus, E, and Poisson ratio, ν, through the following equations

$$K = \frac{E}{3(1-2\nu)} . \tag{4}$$

$$\mathrm{G} = \frac{E}{2(1+\nu)} . \tag{5}$$

The Drucker–Prager model with non-associated plastic flow rules is adopted here. The yield condition $f(I_1,J_2)$ and plastic potential function $g(I_1,J_2)$ have the following forms, respectively

$$f(I_1,J_2)=\sqrt{J_2}+\alpha_\varphi I_1-k_c=0\,. \tag{6}$$

$$g(I_1,J_2)=\sqrt{J_2}+\alpha_\psi I_1-C\,. \tag{7}$$

where I_1 and J_2 are, respectively, the first and second invariants of the stress tensor; C is an arbitrary constant; α_φ and k_c are Drucker–Prager's constants, which are related to the Coulomb's material constants c (cohesion) and φ (internal friction); α_ψ has the same expression as α_φ and is related to the dilatancy angle ψ of geo-materials.

$$\alpha_\varphi=\frac{\tan\varphi}{\sqrt{9+12\tan^2\varphi}},\quad k_c=\frac{3c}{\sqrt{9+12\tan^2\varphi}},\quad \alpha_\psi=\frac{\tan\psi}{\sqrt{9+12\tan^2\psi}}\,. \tag{8}$$

for the 2D plane strain condition

$$\alpha_\varphi=\frac{2\sin\varphi}{\sqrt{3}(3-\sin\varphi)},\quad k_c=\frac{6c\cos\varphi}{\sqrt{3}(3-\sin\varphi)},\quad \alpha_\psi=\frac{2\sin\psi}{\sqrt{3}(3-\sin\psi)}\,. \tag{9}$$

A stress rate that is invariant with respect to rigid-body rotation must be employed for the constitutive relations when considering a large deformation problem. The Jaumann rate of Cauchy stress is used here

$$\dot{\sigma}_J^{\alpha\beta}=\dot{\sigma}^{\alpha\beta}-\dot{\omega}^{\alpha\gamma}\cdot\sigma^{\gamma\beta}-\dot{\omega}^{\beta\gamma}\cdot\sigma^{\alpha\gamma}\,. \tag{10}$$

where '·' denotes the derivative with respect to time; subscript J designates the Jaumann rate; and $\dot{\omega}$ is the spin rate tensor

The final form of the stress–strain relationship for elasto-plastic stress of soil grains can be expressed as

$$\frac{D\sigma_{epi}{}^{\alpha\beta}}{Dt}=\sigma_{epi}{}^{\alpha\gamma}\dot{\omega}^{\beta\gamma}+\sigma_{epi}{}^{\gamma\beta}\dot{\omega}_i^{\alpha\gamma}+2G\dot{e}_i^{\alpha\beta}+K\varepsilon_i^{\gamma\gamma}\delta_i^{\alpha\beta}-\dot{\lambda}_i\left[3\alpha_\psi K\delta^{\alpha\beta}+\frac{G}{\sqrt{J_2}}s_i^{\alpha\beta}\right]. \tag{11}$$

When the granular motion enter into post-failure stage, the viscous stress is dominant. Although the μ(I) rheology was proven to be a robust constitutive relation in granular liquid regime, it was found that a constant viscous rheology also could be applied to well reproduce dynamics and deposit of collapsing granular columns [Ionescu et al. 2015]. This is crucial for practical application to natural flows, because small viscosities involved in μ(I) rheology may induce prohibitive computational time. The artificial viscosity in SPH method was often regarded as an unphysical parameter, however, it can be an alternative to describe granular motion in granular liquid like regime. So the artificial viscosity term is used here not only to stabilise the numerical system, but also to control the granular motion in granular liquid like regime. The concrete expression of viscosity term is described in section 2.2.

2.2. *SPH numerical implementation*

The elasto-plastic viscous implementation with Drucker-Prager yield criterion for solid stage and constant viscosity rheology for fluid stage is developed based on DualSPHysics. The discretized form of mass and momentum conservation equations can be expressed by

$$\frac{D\rho_i}{Dt} = \sum_{j=1}^{N} m_j (v_i^\alpha - v_j^\alpha) \frac{\partial W_{ij}}{\partial x_i^\alpha} . \tag{12}$$

$$\frac{Dv_i^\alpha}{Dt} = \sum_{j=1}^{N} m_j \left(\frac{\boldsymbol{\sigma}_i^{\alpha\beta} + \boldsymbol{\sigma}_j^{\alpha\beta}}{\rho_i \rho_j} - \boldsymbol{\Pi}_{ij} \delta^{\alpha\beta} + F_{ij}^n \mathbf{R}_{ij}^{\alpha\beta} \right) \frac{\partial W_{ij}}{\partial x_i^\beta} + g^\alpha . \tag{13}$$

The strain rate tensor and spin rate tensor used to compute elasto-plastic stress are discretized as

$$\dot{\boldsymbol{\varepsilon}}_i^{\alpha\beta} = \frac{1}{2} \left[\sum_{j=1}^{N} \frac{m_j}{\rho_j} (v_i^\alpha - v_j^\alpha) \frac{\partial W_{ij}}{\partial x_i^\beta} + \sum_{j=1}^{N} \frac{m_j}{\rho_j} (v_j^\beta - v_i^\beta) \frac{\partial W_{ij}}{\partial x_i^\alpha} \right] . \tag{14}$$

$$\dot{\boldsymbol{\omega}}_i^{\alpha\beta} = \frac{1}{2} \left[\sum_{j=1}^{N} \frac{m_j}{\rho_j} (v_i^\alpha - v_j^\alpha) \frac{\partial W_{ij}}{\partial x_i^\beta} - \sum_{j=1}^{N} \frac{m_j}{\rho_j} (v_j^\beta - v_i^\beta) \frac{\partial W_{ij}}{\partial x_i^\alpha} \right] . \tag{15}$$

W_{ij} is the kernel function. The kernel function proposed by Yang and Liu [2012] is used in this study instead of classical kernel functions included in DualSPHysics to suppress the tension instability in the calculation. Its second derivative is non-negative

$$W = (r,h) = \alpha_D \begin{cases} q^3 - 6q + 6, & 0 \le \mathrm{q} < 1 \\ (2-q)^3, & 1 \le \mathrm{q} < 2 \\ 0, & \mathrm{q} \ge 2 \end{cases} \quad \mathrm{q} = \frac{r}{h} . \tag{16}$$

where the normalised coefficient α_D is $1/(3\pi h^2)$ and $15/(62\pi h^3)$ in the 2D and 3D condition respectively, r is the distance between two particles, h is the smoothing length.

The viscous term is given follow Monaghan [1989]

$$\prod_{ij} = \frac{-\alpha \bar{c}_{ij} \mu_{ij}}{\bar{\rho}_{ij}} ; \quad v_{ij} \cdot x_{ij} < 0 . \tag{17}$$

Where $\mu_{ij} = (h_{ij} \cdot v_{ij} \cdot r_{ij}) / (r_{ij}^2 + 0.01 h_{ij}^2)$; $\bar{\rho}_{ij} = (\rho_i + \rho_j)/2$; $\bar{c}_{ij} = (c_{si} + c_{sj})/2$; $h_{ij} = (h_i + h_j)/2$; $v_{ij} = v_i - v_j$; $r_{ij} = r_i - r_j$; $c_s = \sqrt{4G/3\rho + K/\rho}$; α is constant and contingent upon specific problems.

$F_{ij}^n \mathbf{R}_{ij}^{\alpha\beta}$ in Eq. (13) is artificial stress term which is used to reduce tensile instability, where the coefficient $F_{ij} = W_{ij} / W(\Delta x, h)$ and the exponent $n = W(0,h) / W(\Delta x, h)$ are

used to control the value of artificial stress, we set n to 2.55 in this study. And $\mathbf{R}_{ij}^{\alpha\beta} = \mathbf{R}_i^{\alpha\beta} + \mathbf{R}_j^{\alpha\beta}$ here, where $\mathbf{R}_i^{\alpha\beta}$ and $\mathbf{R}_j^{\alpha\beta}$ are the components of the artificial stress tensor at particles *i* and particle *j*. The unify expression for 2D and 3D artificial stress is derived here. Assuming $\boldsymbol{\sigma}\mathbf{x} = \eta\mathbf{x}$, where η is invariant and $\mathbf{x}$ is a non-zero *m*-dimensional vector, then $\eta_1, \eta_2, \ldots \eta_m$ are eigenvalues corresponding to vector $\mathbf{x}$. $\boldsymbol{\sigma}' = diag(\eta_1, \eta_2, \ldots \eta_m)$, *m*=2 for the 2D condition and *m*=3 for condition.

$$\mathbf{R}^{\alpha\beta} = \begin{cases} -\varepsilon \dfrac{\boldsymbol{\sigma}'^{\alpha\beta}}{\rho^2} & \boldsymbol{\sigma}'^{\alpha\beta} > 0 \\ 0 & \boldsymbol{\sigma}'^{\alpha\beta} \le 0 \end{cases}. \tag{18}$$

where the constant ε is taken to be 0.3 after careful calibration.

3. Model Validation

3.1. *Granular column collapse*

The granular column collapse is a classical problem to investigate different regimes of granular flows and transition between them. It contains granular solid regime and granular liquid regime at the same time. So it is an appropriate problem to examine our numerical model. The experiments carried by Bui et al. [2008] and Mangeney et al. [2010] are simulated to verify the ability of the model to reproduce the final deposit and shape evolution of collapsing granular columns on both horizontal and inclined plane. The details of those two experiments can be found in their original papers and are not described here for brevity. To get detailed comparison of dynamics between numerical results and experimental data, we do our own granular column collapse experiment. The experiments are carried out in transparent glass box which has a length of 1m, a height of 0.3m and a width of 0.05m. The initial granular pile is formed behind a glass plate in the right part of the box. The granular pile has dimensions(L,H,W), where L is the length of the pile, H is the Height, W is the width. We keep the W unchanged and vary the L, H in experiments. When the experiment begins, the glass plate is removed away suddenly from the granular pile, and the granular pile begins to collapse. The time for the glass plate to leave t_l is short compared to the time for granular column collapse t_c ($t_l/t_c \approx 1/20$), so we ignore the glass plate in numerical simulation. A high speed camera is used to record the whole process with a speed of 8000 frames per second. The experiment was repeated for three times to exam the experimental repeatability.

The granular media we used is quartz sand. The Young's module E and Poisson's ratio of the quartz sand is 77.8GPa and 0.17, respectively, and its friction angle φ is about 36°. The granular density ρ_s is 2200 kg/m3 and volume fraction ϕ is kept about 0.57 in all experiments. The diameter of the granular media ranged from 20 mesh to 40 mesh. It has been proven that the boundary effect of a channel can be ignored if $\bar{d}/W < 1/20$ where $\bar{d}$ is the mean particle diameter [Jiang et al. (2015)]. In our experiments, $\bar{d}/W \approx 1/90$ which enabled the lateral walls effect to be safely ignored. 5% dyed quartz

Table 1. Properties of granular material used in simulations of different experiments.

Properties	Bui's	Mangeney's	Nguyen's
Density ρ (kg/m^3)	2080	1550	2040
Internal friction angle φ (°)	19.8	25.5	21.9
Cohesion c (MPa)	0	0	0
Poisson's ratio υ	0.3	-	0.3
Elastic modulus E (MPa)	0.7	-	5.84

Table 2. Some details about numerical setup.

Parameters	Bui's	Mangeney's	Nguyen's
Total particle number	15500	49958	23372
Boundary particle number	2700	6208	3372
The ratio between smooth length and particle spacing	1.0	1.0	1.0
Viscous parameter α	0.1	0.05	0.05; 0.1

sand in each experiment was added to do DIC. The Ncorr Software was used to get the velocity profiles.

3.2. *Numerical results*

3.2.1. *Comparison with experiments*

The most parameters used in the numerical model are taken from experimental measurements, just as present in Table 1. And some details about numerical setup are listed in Table 2. Because the constant viscosity are employed instead of the μ(I) rheology, which depends on pressure and strain rate tensor, the values of viscosity has to be calibrated. The calibrated viscosities in different experiments are also include in Table 2. The influence of viscosity will be discussed in section 3.2.2.

Firstly, the comparison of final deposit between simulation and Bui's experiment [Bui et al. (2008)] exhibits good agreement as presented in Fig. 1. It can also be found that the field of accumulated deviatoric plastic strain (ADPS) is very similar to the simulation of Bui [2008]. To further test the ability of the numerical model to reproduce the shape evolution of granular flow on inclined topography, we choose the experiment of granular column collapsing on a plane inclined at an angle of 16 degrees with the horizontal to simulate [Mangeney et al. (2010)]. The results are shown in Fig. 2, from which we can see our simulated results are very similar to Ionescu's [2015]. Although there are some disagreements between simulation and experiment, it has been proven that this is mainly

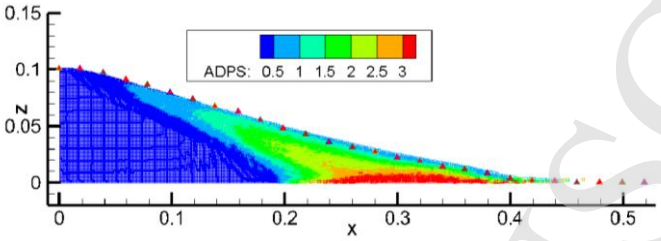

Fig. 1. Comparison of final deposit between Bui's experiment and simulation.

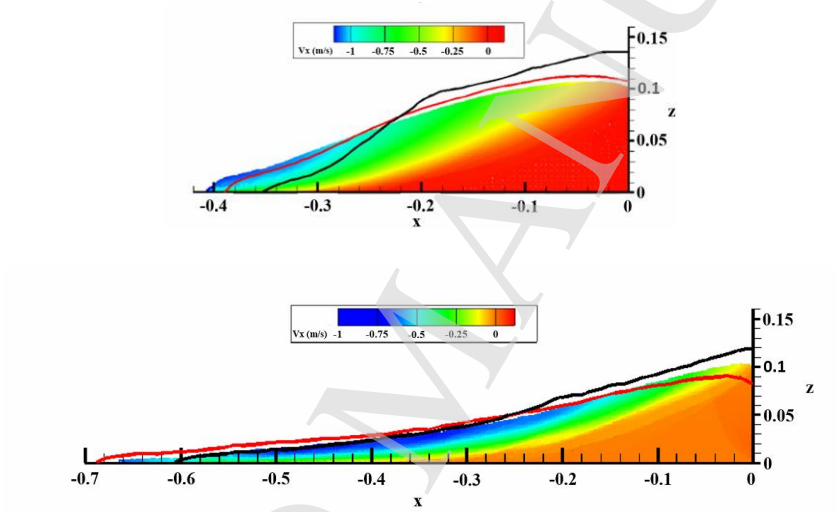

Fig. 2. Shape evolution of granular flow on inclined topography at time t=0.24 sec (top) and t=0.48 sec (bottom). The black curves are the profile in Mangeney's experiment [Mangeney et al. (2010)], the red curves are the simulated results of Ionescu [Ionescu et al. (2015)].

due to the two dimensional simulations ignore lateral wall effects which it is crucial when granular collapses on slope $\geq 10°$ [Martin et al. (2017)]. However, it is hard to include lateral wall effects in two dimensional simulations by a simple method when granular avalanche along complex topography. Thus, it is important to adopt three dimensional simulation in natural granular avalanche along channel. Previous numerical methods have focused on reproduction of scaling laws, final deposit and shape evolution for granular collapse [Kerswell (2005); Hu et al. (2018); Martin et al. (2017)], few quantitative

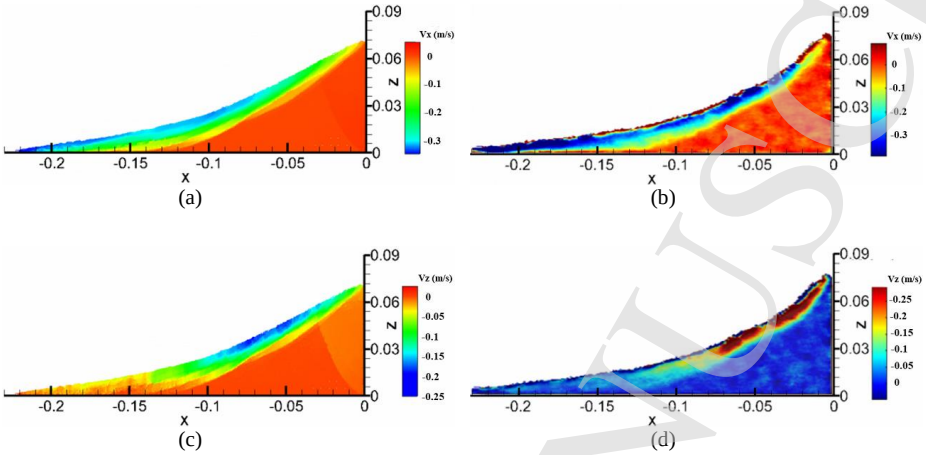

Fig. 3. Comparison of velocity of our experimental and numerical results at t=0.3s. (a) and (c) show velocity of x direction and z direction in numerical modeling. (b) and (d) show velocity of x direction and z direction in experiment.

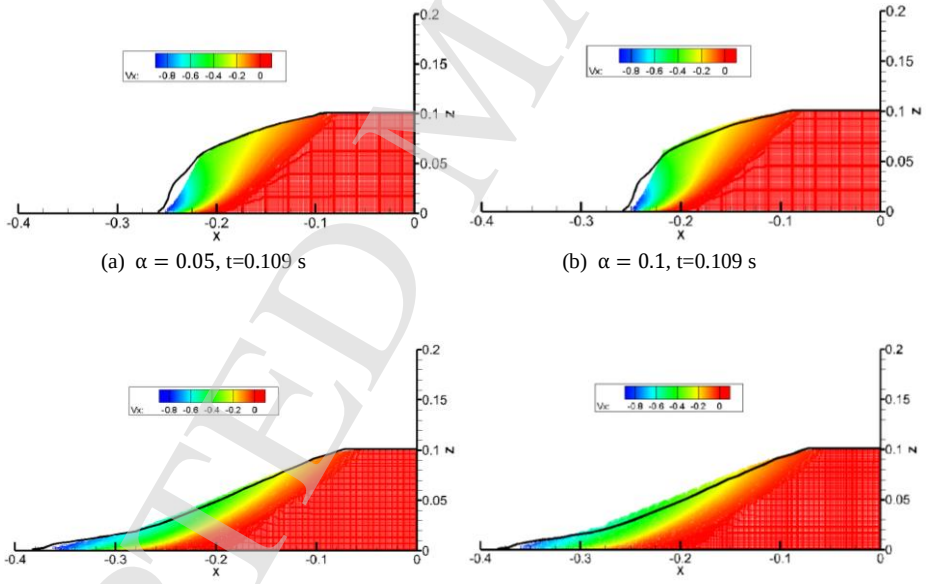

Fig. 4. Effect of viscous term on the flow process at time t=0.109 sec (top) and t=0.235 sec (bottom). Black curves are the profile in the experiment of Nguyen [2015].

comparisons have been made between experiment and simulation for detailed velocity field. We choose an experiment where $H = 0.12$ m and $L = 0.05$m to simulate. A time at the experiment is randomly selected for comparison of velocity field between simulate

result and experimental data. As we can see from Fig. 3, the flow region and the magnitude of velocity show only slight differences between simulation and experiment.

3.2.2. *Effect of viscosity*

We simulate the experiment of Nguyen [2015] by using different viscous value to test the influence of viscosity. From Fig. 4, it could be found that the viscosity has little influence on dynamics of granular column collapse at t=0.109s just as the work of Mao et al [2017]. This means the dissipation due to viscous effect is much smaller than that due to plastic strain when shear velocity is relatively small. However, the viscosity clearly influence the dynamics of granular column collapse at t=0.235s. Thus, it's of great importance to choose an appropriate viscosity in the model. It need to be further investigated whether the spatio-temporal average of the range of values computed using μ(I) rheology is the best value to use in the model and whether it can be measured directly in the experiments [Martin et al. (2017)]. From the simulation, it also could be concluded it is not enough to use a small height-width ratio granular column collapse on horizontal plane where the shear velocity is relatively small as a case to verify a viscoplastic model for granular motion just as the research of Pahar and Dhar [2017].

4. Case Study: The Yigong Avalanche

4.1. *Parameters selection*

An extremely large, high speed rock avalanche occurred on April 9, 2000 at Yigong, Tibet, China, it is the largest avalanche among those wasn't caused by earthquake in recent 100 years. Billions of cubic meters materials travelled up to 10 km, dammed the Yigong River, forming an extensive lake rockslide-dammed lake. The dam failed on 10 June, 2000 and caused significant losses downstream [Delaney and Evans (2015)].

Appropriate selection of model parameters is a key factor to simulate the motion of granular avalanche accurately. The simulation of Yigong avalanche was mostly all based on shallow-type model which need to calibrate model parameter [Xu et al. (2012); Delaney and Evans (2015); Kang et al. (2012); Wang and Li (2017)], while we choose the model parameter carefully.

The effective internal friction of undrained ring shear and drained ring shear test are 19.8° and 36.2° , respectively [Hu et al. (2009)]. It can be inferred that pore pressure is hard to accumulate through the grain size distributions of fine particles sample and material compositional description of Yigong avalanche [Kang et al. (2016); Zhou et al. (2016)]. Thus, the effective internal friction get through drained ring shear may be more representative. However, the landslide stops very quickly if we adopt 36.2° in the simulation. Therefore, there must be some mechanism cause the friction angle to reduce in the avalanche process. Lucas et al. [2014] concluded that basal frictional angle would decrease through a large collection of data, and they proposed an empirical velocity-weaken friction law

$$\mu(U) = \frac{\mu_0 - \mu_w}{(1 + \|U\| / U_w)} + \mu_w . \tag{18}$$

with $\mu_w = 0.11$ and $U_w = 4m \cdot s^{-1}$, where μ_0 and μ_w are static and velocity-weakening friction coefficient, respectively, $\|U\|$ represents slip velocity and U_w is a characteristic velocity for the onset of velocity-weakening. The value of μ_0 is 0.74 for Yigong avalanche. The Yigong avalanche accelerated to high speed in very short time and kept high-speed moving before striking south bank of the Yigong river. The Yigong avalanche travelled up to 10 km in two to three minutes, thus, the mean velocity of it would be 83.3 m/s to 55.5 m/s, then we can get the basal friction coefficient of Yigong avalanche is in the range of 0.138 to 0.152 by applying Eq. (18).

Recently, Wang et al. [2017] carried out rotary shear experiments at velocities ranging from 0.07m/s to 1.31 m/s and at normal stress about the basal stress of the Yigong avalanche by using soil sample taken from basal facies of the Yigong avalanche, they found there are apparent frictional weakening when shear velocity exceed 0.15 m/s. They also proposed an empirical equation for frictional coefficient of Yigong avalanche basal friction.

$$\mu(U) = 0.13 + 0.6e^{-4.72\|U\|} \quad (\|U\| > 0.15m/s) . \tag{19}$$

The frictional coefficient is very close to 0.13 once the magnitude of shear velocity higher than 0.87 m/s, which is very close to the estimated value by using Eq. (19).

Just as mentioned before, Yigong avalanche accelerated to high speed in very short time and kept high-speed moving, so the basal frictional coefficient reached the steady value, 0.13, very quickly. However, it is hard to estimate the intensity of shear rate inside the avalanche body directly. Perinotto et al. [2015] found there are particle fragment and fluidization effect in the inner part of avalanche just as on the basal face. Thus, the frictional angle is set to 7.4°, which is the value of $\arctan 0.13$. 38.1 KPa is chosen as cohesion according to the measurement of Hu et al. [2009]. Other soil parameters needed in the model is set to characteristic value.

The elevation data of NASA's global digital elevation model (GDEM) is used in this study. The distribution of source mass is roughly estimated according to the topography change of Zhamu Creek before and after 2000 Yigong avalanche. The initial state of soil is achieved by simulating with very large values of friction angle and cohesion long enough. Then the friction angle and cohesion are changed to true values suddenly, source mass begins to collapse. In the simulation of Yigong avalanche, there are about 2.87 million SPH particles in total, and 68132 particles are used to fill in the landslide mass. The no-slip boundary conditions in enforced in this simulation, details of the implementation of this boundary conditions in SPH can be found in Bui et al. [2008].

4.2. *Comparison with site survey*

We compare our numerical result in both time and space. Although there was no detailed time data of the Yigong avalanche due to its emergency, we can infer it last about 6 minutes from recorded seismic wave, and the seismic wave recorded at Linzhi seismostation indicate the time of active vibration is about two minutes [Ren et al. (2001)]. We show our simulate result of Yigong avalanche at two minutes, three minutes and five minutes in Fig. 5. From the results, it could be find that the avalanche impacts on south bank of the Yigong river at about two minutes and slows down quickly. This phenomenon not only match well with the recorded seismic wave, but also consistent with the observation that

the mass movement still had a high speed when crossing the Yigong River valley [Xu et al. (2012)]. And the Fig. 5 (c) show the granular avalanche stops completely at five to six minutes, which agree with site observation too. As for spatial scale, the comparison of debris distribution between simulated result and site survey in Fig. 6 is satisfactory.

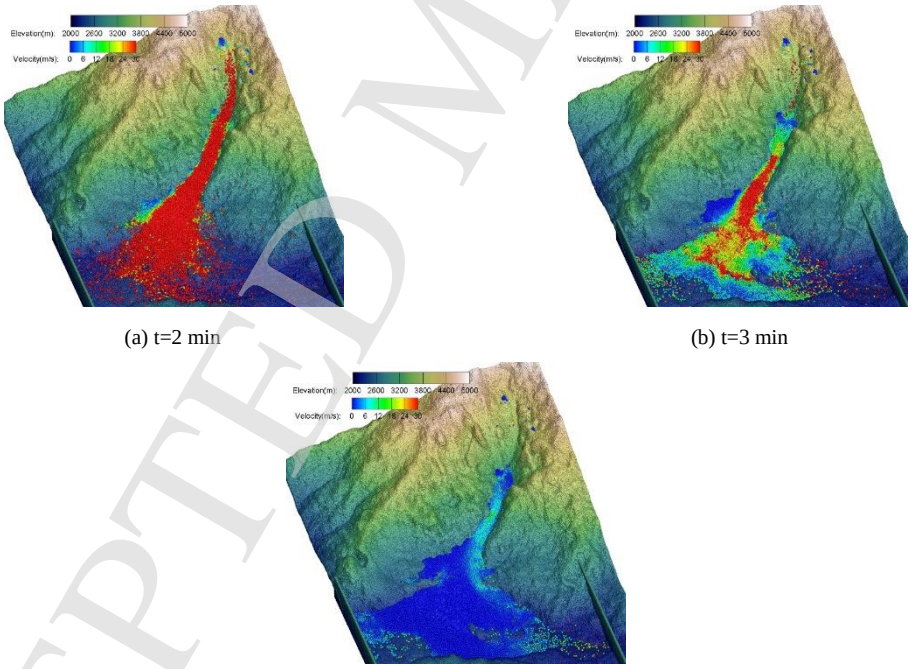

(a) t=2 min (b) t=3 min

(c) t=5min

Fig. 5. Outputs from the SPH simulation of Yigong avalanche at three different time step.

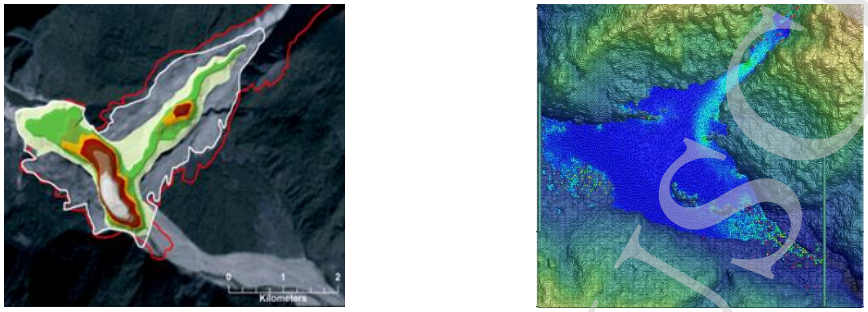

Fig. 6. The comparison of final deposit of Yigong avalanche between field survey and simulation

5. Conclusion

An effective numerical model for avalanche plays important role in landslide hazard assessment and hazards prevention. This study develops a numerical model based on three-dimensional continuum equations, which take granular material's constitutive relation in different stage of granular avalanche into consideration. The Drucker–Prager model with non-associated plastic flow rules is adopt for granular solid-like regime and constant viscosity rheology is employed for granular liquid-like regime. The governing equations are discretised into SPH framework based on DualSPHysics. The granular column collapse is a classical problem which contains granular solid regime and granular liquid regime at the same time. We got good agreement on both the shape evolution and the velocity field when using our elasto-plastic viscous model to simulate granular collapse experiment.

We simulated the high-speed and long-distance Yigong avalanche as a case study, then found the propagation distance in the simulation would be very short if the friction angle measured through classical drained shear test is employed. Therefore, there must be certain mechanism caused the significant reduction of friction angle. We set the frictional angle to the value measured through high speed shear experiment after same discussion, then the time of duration, deposited scope and estimated velocity match well with site survey.

However, the numerical model can be developed further. For example, it may be better to employ the μ(I) rheology in granular fluid-like regime since it doesn't need to calibrate viscosity. Moreover, the size segregation, granular fragment and soil erosion need to be considered in the future.

Acknowledgments

This work was financially supported by the National Natural Science Foundation of China (No. 11672310, No. 11432015) and the National Basic Research Program of China (No. 2014 CB04680202).

References

Andrade, J. E., et al. (2012). On the rheology of dilative granular media: bridging solid-and fluid-like behavior. J. Mech. Phys. Solids, 60(6): 1122–1136.

Bui, H. H., et al. (2008). Lagrangian meshfree particles method (SPH) for large deformation and failure flows of geomaterial using elastic–plastic soil constitutive model. Int. J. Numer. Analyt. Methods Geomech., 32(12): 1537–1570.

Chen, W. and Qiu, T. (2014). Simulation of earthquake-induced slope deformation using SPH method. Int. J. Numer. Analyt. Methods Geomech., 38(3): 297–330.

Davies, T. R. H., McSaveney M. J. and Hodgson K. A. (1999). A fragmentation-spreading model for long-runout rock avalanches. Can. Geotech. J., 36(6): 1096–1110.

Delaney, K. B. and Evans, S. G. (2015). The 2000 Yigong landslide (Tibetan Plateau), rockslide-dammed lake and outburst flood: Review, remote sensing analysis, and process modelling. Geomorphology, 246: 377–393.

Denlinger, R. P. and Iverson, R. M. (2004). Granular avalanches across irregular three-dimensional terrain: 1. Theory and computation. J. Geophys. Res., 109: F01014.

Dunatunga, S. and Kamrin, K. (2015). Continuum modelling and simulation of granular flows through their many phases. J. Fluid Mech., 779:483–513.

Garg, S. and Pant, M. (2018). Meshfree Methods: A Comprehensive Review of Applications. Int. J. Comput. Methods, 15(3): 1830001.

Gray, J. M. N. T. and Edwards, A. N. (2014). A depth-averaged μ(I)-rheology for shallow granular free-surface flows. J. Fluid Mech., 755: 503–534.

Griffiths, D. V. and Marquez, R. M. (2007). Three-dimensional slope stability analysis by elasto-plastic finite elements. Géotechnique, 57(6): 537–546.

Holsapple, K. A. (2013). Modeling granular material flows: the angle of repose, fluidization and the cliff collapse problem. Planet. Space Sci., 82: 11–26.

Hu, M., et al. (2015). Three-dimensional run-out analysis and prediction of flow-like landslides using smoothed particle hydrodynamics. Environ. Earth Sci., 73(4): 1629–1640.

Hu, M., et al. (2018). GIS Enabled SPH-Soil Modeling for the Post-Failure Flow of Landslides Under Seismic Loadings. Int. J. Comput. Methods, 15(3): 1850046.

Hu, M. J., Cheng, Q. G. and Wang, F. W. (2009). Experimental study on formation of Yigong long-distance high-speed landslide. Chin. J. Rock Mech. Eng., 28(1): 138-143 (In Chinese).

Huang, J., Leebeeck, A. D. and Nydal, O. J. (2012). Simulations of particulate flows using multi-scale time steps. Int. J. Comput. Methods, 9(1): 1240010.

Huang, Y., et al. (2012). Run-out analysis of flow-like landslides triggered by the Ms 8.0 2008 Wenchuan Earthquake using smoothed particle hydrodynamics. Landslides, 9(2): 275–283.

Ionescu, I. R., et al. (2015). Viscoplastic modeling of granular column collapse with pressure-dependent rheology. J. Non-Newtonian Fluid Mech., 219: 1–18.

Iverson, R. M. (1997). The physics of debris flows. Rev. Geophys., 35: 245–296.

Jiang, Y. J., et al. (2015). Influence of particle characteristics on impact event of dry granular flow. Powder Technol., 270: 53–67.

Kang, C., et al. (2016). Runout and entrainment analysis of an extremely large rock avalanche—a case study of Yigong, Tibet, China. Landslides, 14(1): 1-17.

Kerswell, R. R. (2005). Dam break with Coulomb friction: A model for granular slumping. Phys. Fluids 17: 057101.

Lucas, A., Mangeney, A. and Ampuero, J. P. (2014). Frictional velocity-weakening in landslides on Earth and on other planetary bodies. Nature Communs., 5: 3417.

Mangeney, A., et al. (2010). Erosion and mobility in granular collapse over sloping beds. J. Geophys. Res.: Earth Surf., 115: F03040.

Mao, Z. R., Liu, G. R. and Dong, X. W. (2017). A comprehensive study on the parameters setting in smoothed particle hydrodynamics (SPH) method applied to hydrodynamics problems. Comput. Geotech: 92: 77-95.

Martin, N., et al. (2017). Continuum viscoplastic simulation of a granular column collapse on large slopes: μ(I) rheology and lateral wall effects. Phys. Fluids, 29: 013301.

Melosh, H. J. (1979). Acoustic fluidization: a new geologic process? J. Geophys. Res., 84: 7513–7520.

Monaghan, J. J. (1989). On the problem of penetration in particle methods. J. Comp. Phys., 82(1): 1-15.

Nguyen, C. T., Bui, H. H and Bui, F R (2015). Failure mechanism of 2D granular flows: experiment. J. Chem. Eng. Jpn., 48(6): 395–402.

Pahar, G. and Dhar, A. (2017). Coupled incompressible Smoothed Particle Hydrodynamics model for continuum-based modelling sediment transport. Adv. Water Resour., 102: 84-98.

Perinotto, H. (2015). The extreme mobility of debris avalanches: A new model of transport mechanism. J. Geophys. Res. Solid Earth, 120: 8110–8119.

Ren, J.W., et al. (2001). Geological characteristic sand kinematics of the rock fall-landslide in Yigong, Southeastern Tibet. Geol. Rev., 47(6): 642–647 (In Chinese).

Wang, X. L. and Li, J. C. (2017). A new solver for granular avalanche simulation: Indoor experiment verification and field scale case study. Sci. China Phys. Mech. Astron., 60: 124712.

Wang, Y. F., Dong, J. J. and Cheng, Q. G. (2017). Velocity-dependent frictional weakening of large rock avalanche basal facies: Implications for rock avalanche hypermobility?. J. Geophys. Res. Solid Earth, 122: 1648–1676.

Xu, Q., et al. (2012). Observations from the large, rapid Yigong rock slide-debris avalanche, southeast Tibet. Can. Geotech. J., 49: 589–606.

Xu, T. B., et al. (2017). Simulation of velocity and shear stress distributions in granular column collapses by a mesh-free method. J. Non-Newtonian Fluid Mech., 247: 146-164.

Yang, X. F. and Liu, M. B. (2012). Improvement on stress instability in smoothed particle hydrodynamics. Acta Phys. Sin., 61(22): 224701 (in Chinese).

Zhang, Y. B., et al. (2013). Effects of geometries on three-dimensional slope stability. Can. Geotech. J. , 50(3): 233–249.

Zhou, J. W., Cui, P. and Hao, M. H. (2015). Comprehensive analyses of the initiation and entrainment processes of the 2000 Yigong catastrophic landslide in Tibet, China. Landslides, 13(1): 39–54.